RNA BIOLOGY
2019, VOL. 16, NO. 3, 295–308
https://doi.org/10.1080/15476286.2019.1572436

Taylor & Francis
Taylor & Francis Group

RESEARCH PAPER

OPEN ACCESS Check for updates

Direct visualization of the native structure of viroid RNAs at single-molecule resolution by atomic force microscopy

M. Moreno [a], L. Vázquez [b], A. López-Carrasco [c], J.A. Martín-Gago [b], R. Flores [c], and C. Briones [a,d]

[a]Department of Molecular Evolution, Centro de Astrobiología (CSIC-INTA), Torrejón de Ardoz, Madrid, Spain; [b]Departamento de Superficies y Recubrimientos, Materials Science Factory, Instituto de Ciencia de Materiales de Madrid (CSIC), Cantoblanco, Madrid, Spain; [c]Instituto de Biología Molecular y Celular de Plantas (CSIC-UPV), Valencia, Spain; [d]Centro de Investigación Biomédica en Red de enfermedades hepáticas y digestivas (CIBERehd), Spain

ABSTRACT

Viroids are small infectious, non-protein-coding circular RNAs that replicate independently and, in some cases, incite diseases in plants. They are classified into two families: *Pospiviroidae*, composed of species that have a central conserved region (CCR) and replicate in the cell nucleus, and *Avsunviroidae*, containing species that lack a CCR and whose multimeric replicative intermediates of either polarity generated in plastids self-cleave through hammerhead ribozymes. The compact, rod-like or branched, secondary structures of viroid RNAs have been predicted by RNA folding algorithms and further examined using different *in vitro* and *in vivo* experimental techniques. However, direct data about their native tertiary structure remain scarce. Here we have applied atomic force microscopy (AFM) to image at single-molecule resolution different variant RNAs of three representative viroids: potato spindle tuber viroid (PSTVd, family *Pospiviroidae)*, peach latent mosaic viroid and eggplant latent viroid (PLMVd and ELVd, family *Avsunviroidae)*. Our results provide a direct visualization of their native, three-dimensional conformations at 0 and 4 mM Mg^{2+} and highlight the role that some elements of tertiary structure play in their stabilization. The AFM images show that addition of 4 mM Mg^{2+} to the folding buffer results in a size contraction in PSTVd and ELVd, as well as in PLMVd when the kissing-loop interaction that stabilizes its 3D structure is preserved.

ARTICLE HISTORY
Received 26 July 2018
Revised 11 December 2018
Accepted 17 January 2019

KEYWORDS
Viroids; RNA structure; RNA structural/functional elements; kissing-loop interactions; ribozymes; atomic force microscopy; single-molecule approaches

Introduction

Viroids are the smallest known nucleic acid-based infectious agents, with their genomes consisting of a single-stranded (ss), circular, non-protein-coding RNA ranging in size from ~250 to 430 nucleotides (nt) [1–5]. Viroids replicate and invade systemically some host plants, often causing disease by altering pathways that mediate gene expression and development [6–10]. Viroid replication takes place in the nuclei (family *Pospiviroidae)* or in plastids, mostly chloroplasts (family *Avsunviroidae*), and proceeds through an entirely RNA-based rolling-circle mechanism [11–16]. In the best supported model [17] the infecting, most abundant monomeric circular *(mc)* strand, to which the (+) polarity is assigned by convention, is reiteratively transcribed by either the nuclear RNA polymerase II or a nuclear-encoded chloroplastic RNA polymerase (both redirected to accept RNA templates), thus producing multimeric (-) strands. In the family *Pospiviroidae* the latter serve directly as templates for generating multimeric (+) strands that are cleaved, within a central conserved region (CCR), into unit-length monomeric linear *(ml)* forms by an RNase of class III, and then circularized by DNA ligase 1 (redirected to accept RNA substrates). In the family *Avsunviroidae* the multimeric (-) strands are first cleaved by embedded hammerhead ribozymes, with a chloroplastic isoform of tRNA ligase catalyzing circularization of the resulting *ml* (-) into the *mc* (-) forms which, in turn, prime the second half of the replication cycle that is symmetric to the first one. Due to the presence of ribozymes, along with other properties (see below), viroids have been proposed to be relics of the RNA world [17,18] in the context of the origin and early evolution of life [19].

Data derived from different approaches support the notion that viroid RNA genomes are largely self-complementary, folding into highly-compact rod-shaped or branched secondary structures composed of double-stranded (ds) RNA stretches flanked by internal loops and bulges that are often stabilized by non-canonical interactions [20,21]. Potato spindle tuber viroid (PSTVd, 359 nt), the type member of the family *Pospiviroidae* [22,23], adopts a predicted rod-like secondary structure *in silico, in vitro* and *in vivo* [23–26]. Its terminal and internal loops, as well as the bulges, are critical for replication and systemic trafficking throughout the infected plant [27–30]. In contrast, members of the family *Avsunviroidae*, like peach latent mosaic viroid (PLMVd, 337 nt) [31] and eggplant latent viroid (ELVd, 335 nt) [32], adopt either multibranched or bifurcated secondary structures, respectively. Moreover, in PLMVd and the other member of the genus *Pelamoviroid* [33], the (+) strands are stabilized by

CONTACT C. Briones cbriones@cab.inta-csic.es Department of Molecular Evolution, Centro de Astrobiología (CSIC-INTA), Torrejón de Ardoz, Madrid, Spain
Supplemental data for this article can be accessed here.

a kissing-loop interaction required for *in vitro* folding and *in vivo* viability [34–36].

However, when it comes to single-molecule approaches, data on the three-dimensional (3D) native (or denatured) structures of viroid RNA genomes are very scarce. More specifically, transmission electron microscopy (TEM) has revealed that under non-denaturing conditions PSTVd adopts a ~ 50 nm long, rod-like secondary structure resulting from the high self-complementarity of the viroid RNA [37,38]. Under mild denaturing conditions, besides the 'double-stranded' rods, partially open molecules resembling 'tennis rackets' as well as completely denatured linear and circular single-stranded RNAs were observed [39,40].

Atomic force microscopy (AFM) is a type of scanning probe microscopy that allows structural and dynamic studies of single macromolecules at nanometer resolution [41,42]. One of the main advantages of AFM over electron microscopy-based techniques is that it offers a 3D surface profile of the imaged sample without requiring any staining or coating, thus minimizing structural disruption of the biological entity under study. AFM permits visualization and manipulation across length scales that range from biomolecules to cells. Therefore, this technology is increasingly used in different fields, including virology [43–45]. In particular, AFM has matured to provide nanometer spatial resolution of RNA molecules of different lengths and structures, as well as of RNA-RNA or RNA-protein complexes [46–49]. Within this framework, and based on our previous experience in imaging by AFM structured and functional RNA molecules of viral origin [50], here we have conducted a high resolution structural analysis of the three viroids mentioned above (PSTVd, PLMVd and ELVd), using different variants thereof and experimental conditions. This analysis has allowed the first AFM visualization of the native structures of single viroid RNA molecules, from which functional implications can be derived.

Results

AFM analysis of viroid structure

To investigate the native 3D structure at single-molecule resolution of representative viroid RNAs of the families *Pospiviroidae* (PSTVd) and *Avsunviroidae* (PLMVd and ELVd), a systematic and comparative AFM analysis was performed. RNA adsorption on mica surfaces was performed using 3-aminopropyltriethoxysilane (APTES), one of the currently available reagents that promotes a tight adhesion of RNA molecules via electrostatic interactions without damaging or disrupting their native structure [45,49,50]. Other reported routes for the surface binding of RNA, such as those comprising the addition of salts containing divalent cations (e.g. Mg^{2+}, Zn^{2+} or Ni^{2+}) [45,51,52], are not appropriate for this study given our interest in examining the effect exerted by a divalent cation (Mg^{2+}) on viroid 2D and, particularly, 3D RNA structure.

After RNA thermal denaturation followed by renaturation in the folding buffer lacking Mg^{2+} or in some instances containing 4 mM Mg^{2+}, at least three independent samples of each of the nine viroid RNA preparations (Table 1) were imaged by AFM. Besides the analysis of the shape and main structural features of the imaged viroid RNAs, the average length of 25 individual, full-length molecules from each viroid preparation was computed.

Potato spindle tuber viroid (family Pospiviroidae): a rod- or quasi-rod-shaped structure imaged as consecutive bumps

PSTVd is a 359 nt-long RNA with a theoretical length of approximately 49 nm (assuming a uniform A-dsRNA structure with a pitch of 3.0 nm and 11 bp/turn: 180 bp x 0.27 nm/bp = 48.6 nm) [48,53], resulting in a proposed rod-like secondary structure (Fig. 1A). Two RNAs of this viroid were imaged (Table 1): PSTVd-*ml*(+), the *ml* (+) RNA transcribed *in vitro* (linearized between positions C1 and G2), and PSTVd-*mc*(+), the *mc* (+) RNA isolated from infected plant leaves. The first RNA was renatured in the folding buffer lacking Mg^{2+} or containing 4 mM MgCl$_2$, whereas the second one was only imaged in 4 mM Mg^{2+}-containing buffer. Fig. 1B shows representative 2D and 3D AFM images in ambient conditions of PSTVd-*ml*(+) renatured in buffer without Mg^{2+}, and Suppl. **Fig. S1** depicts 25 single-molecule 2D images together with the measured length of each of them. Their topographic profiles reflect a majority of rod- or quasi-rod-like molecules composed of three consecutive, elongated bumps displaying different angular orientations (with one of the bumps generally forming an angle of 90° to 180° with

Table 1. Main features of the viroid RNAs imaged by AFM in this work.

Family	Viroid	Length (nt)	Variant RNA analyzed (GenBank acc no.)	Features	[Mg^{2+}] in the folding buffer*
Pospiviroidae	PSTVd	359	**PSTVd-*ml*(+)**	*ml* (+) RNA, *in vitro* transcript (IVT)	0
			(U23058.1)		4
			PSTVd-*mc*(+)	*mc* (+) RNA, isolated from infected tissue	4
			(AJ634596.1)		
Avsunviroidae	PLMVd	337	**PLMVd-*ml*(+)wt**	*ml* (+) RNA (wild type), IVT	0
			(AJ005303.1)		4
			PLMVd-*ml*(+)mut	*ml* (+) RNA (mutant with kissing-loop disrupted), IVT	4
	ELVd	335	**ELVd-*ml*(+)**	*ml* (+) RNA, IVT	0
			(AJ536613)		4
			ELVd-*ml*(-)	*ml* (-) RNA, IVT	4
			(AJ536613)		

*The folding buffer is composed of 100 mM HEPES pH 7.4 and 100 mM NaCl, either lacking Mg^{2+} or supplemented with 4 mM MgCl$_2$.

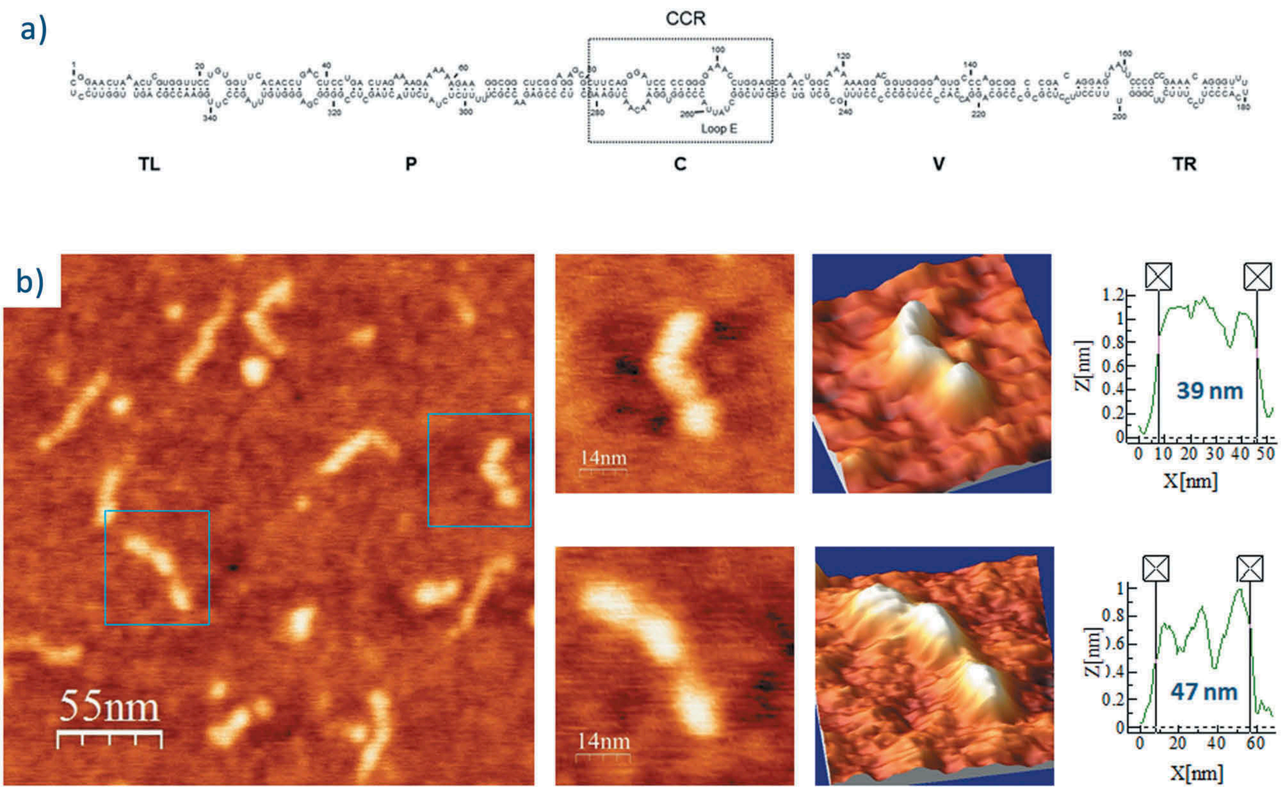

Figure 1. **(A) Predicted secondary structure of PSTVd-*ml*(+).** The 359 nt-long, rod-like secondary structure of PSTVd shows the five domains characteristic of members of the family *Pospiviroidae*: Terminal Left (T_L), Pathogenic (P), Central (C), Variable (V), and Terminal Right (T_R) [77]. The Central Conserved Region (CCR) is located within the C domain and contains an UV-sensitive loop E motif stabilized by non-canonical base-pairs. Adapted from [26]. **(B) AFM images of PSTVd-*ml*(+), renatured in the absence of Mg^{2+}.** A field of 275 × 275 nm is shown on the left panel and two characteristic molecules are zoomed on the right one. 3D views of the imaged viroid RNAs, as well as profiles with their measured lengths (X [nm]) and heights [Z [nm]), are also displayed.

respect to the other two). The bumps might correspond to dsRNA segments flanked by internal loops or bulges; although more than three bumps should be expected according with the number of internal loops or bulges predicted *in vivo* [26], some of them (in particular, the symmetrical or quasi-symmetrical internal loops) might not induce a pronounced bending detectable by AFM.

The average length of PSTVd-*ml*(+), calculated after measuring 25 unbiasedly chosen, full-length viroid molecules present in different preparations (Suppl. **Fig. S1**), was 43 nm (Table 2), being each individual bump 10 to 18 nm long and 0.6 to 1 nm high. In turn, PSTVd-*ml*(+) renatured in the buffer containing 4 mM Mg^{2+} showed a topologically analogous rod-like structure (Fig. 2 and Suppl. **Fig. S2**), but its average length was reduced to 35 nm (18.6% shorter than that of the same viroid RNA in the buffer lacking Mg^{2+}, a statistically significant length reduction as revealed by an ANOVA test, see Table 2), and the internal bumps appeared less clear, thus indicating a Mg^{2+}-induced molecular compaction.

A different form of the same viroid, PSTVd-*mc*(+), the *mc* (+) RNA isolated from infected plant leaves, was purified and AFM imaged after renaturation in 4 mM Mg^{2+}-containing buffer. The imaged rod-like features (Fig. 3 and Suppl. **Fig. S3**) were fairly indistinguishable from those of PSTVd-*ml*(+), thus suggesting that the covalent closing of the molecule occurring *in vivo* did not affect the overall topology of the viroid RNA. Its average molecular length was 35 nm, equivalent to that of PSTVd-*ml*(+) under the same Mg^{2+} concentration.

Table 2. Summary of the average molecular lengths of individual viroid RNAs (n = 25 in all cases) imaged by AFM (shown in Suppl. **Figs S1 to S9**).

Viroid RNA variant	[Mg^{2+}] in the folding buffer	Measured length (nm)		ANOVA test *	
		Mean ± SD	Median	*F*	*F crit*
PSTVd-*ml*(+)	0	43 ± 6*	42.0	15.85	3.12
	4	35 ± 6	35.0		
PSTVd-*mc*(+)	4	35 ± 6	34.7		
PLMVd-*ml*(+)wt	0	34 ± 3	34.3	63.16	3.12
	4	24 ± 4*	24.1		
PLMVd-*ml*(+)mut	4	33 ± 4	33.0		
ELVd-*ml*(+)	0	30 ± 2*	29.6	11.04	3.12
	4	26 ± 5	26.2		
ELVd-*ml*(-)	4	25 ± 4	25.0		

*One-way ANOVA was used to test the null hypothesis that the mean length of the three variants within each viroid species is equal. The results show that *F* > *F crit* in all cases, thus evidencing that the mean length of one of the three variants (marked with an asterisk in the 'Mean' column) is significantly different than those of the other two.

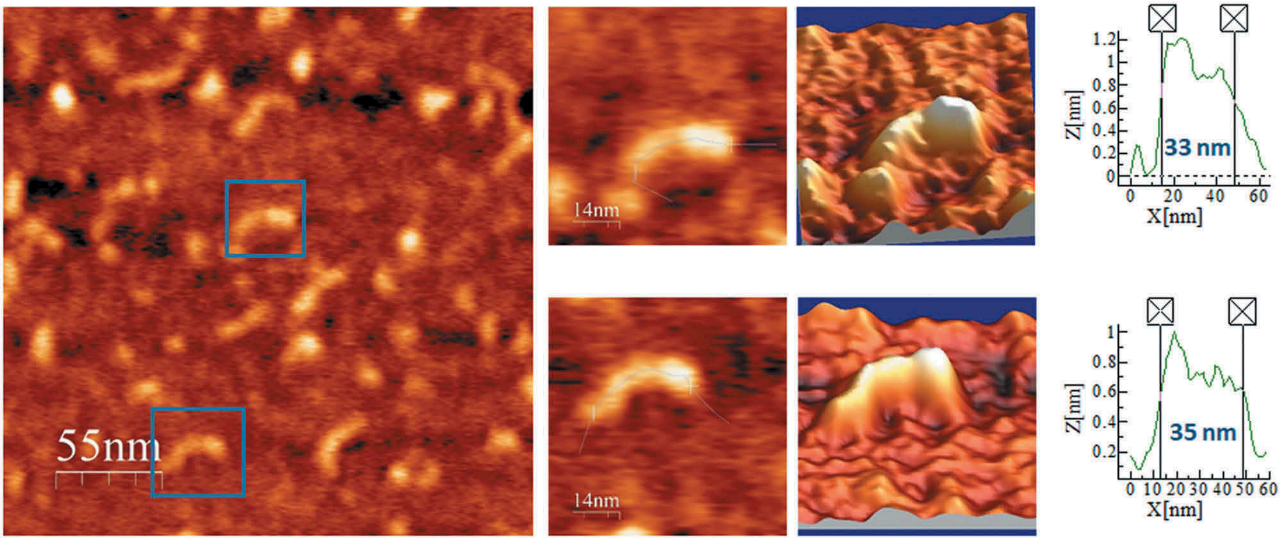

Figure 2. AFM images of PSTVd-*ml*(+) renatured in 4 mM Mg^{2+}. A field of 275 × 275 nm is shown on the left panel and two characteristic molecules are zoomed on the right one. 3D views of the imaged viroid RNAs, as well as profiles with their measured lengths, are also displayed.

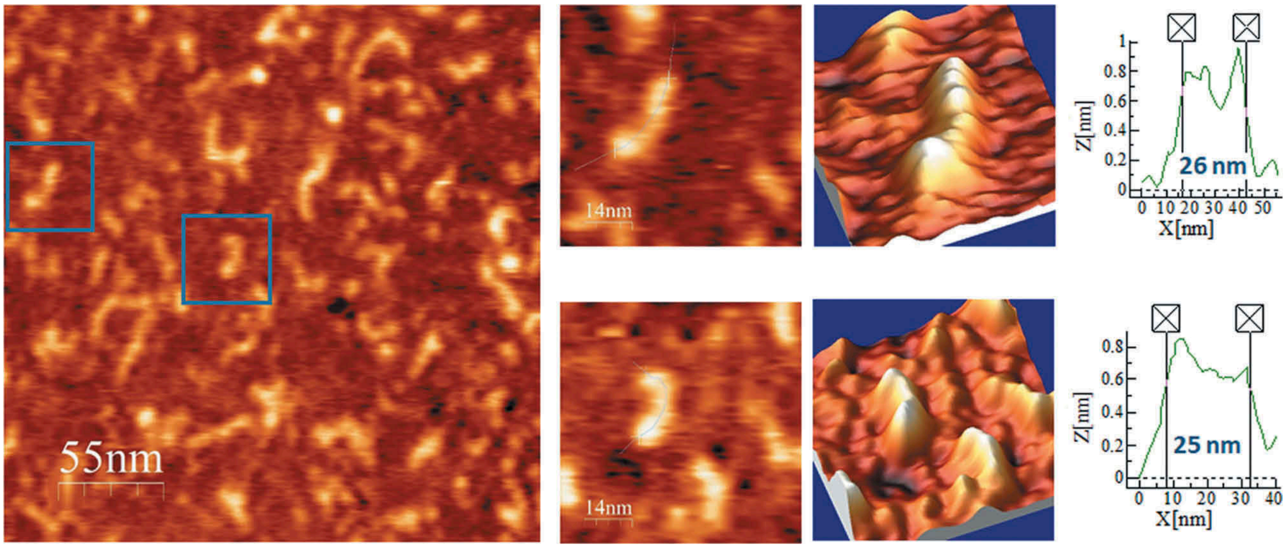

Figure 3. AFM images of PSTVd-*mc*(+) renatured in 4 mM Mg^{2+}. A field of 275 × 275 nm is shown on the left panel and two characteristic molecules are zoomed on the right. 3D views of the imaged viroid RNAs, as well as profiles with their measured lengths, are also displayed.

The size distribution of the imaged variants of PSTVd (depicted in Suppl. **Figs. S1 to S3**) is represented in Fig. 4A. This comparison of viroid lengths at single-molecule level reveals that the most frequently imaged PSTVd-*ml*(+) molecules are 36–40 nm long at 0 mM Mg^{2+}, while the peak in the distribution is shifted to the 31–35 nm interval for both PSTVd-*ml*(+) and PSTVd-*mc*(+) at 4 mM Mg^{2+}. This result reinforces the significant difference in mean lengths shown in Table 2.

Peach latent mosaic viroid (family Avsunviroidae): a kissing-loop interaction critical for stabilizing the 3D structure

Following the same workflow, we performed the AFM imaging of PLMVd-*ml*(+)wt, the wild type *ml* (+) RNA resulting from self-cleavage during *in vitro* transcription of head-to-tail dimeric RNA. The predicted secondary structure of this viroid RNA (Fig. 5A) shows a ramified topology, with a rod-like domain (the so-called 'hammerhead arm', spanning positions 1–53 and 284–337) protruding from a multibranched domain spanning positions 54–283 [54]. This second domain is stabilized by a well-characterized kissing-loop interaction between nucleotides $_{176}\text{GCGG}_{179}$ and $_{209}\text{CCGC}_{212}$ in PLMVd-*ml*(+)wt [34], which is disrupted in the mutant PLMVd-*ml*(+)mut, wherein positions 209–212 are four consecutive As introduced by site-directed mutagenesis. The topographic image of PLMVd-*ml*(+)wt in the folding buffer without added Mg^{2+} (Fig. 5B and Suppl. **Fig. S4**) recalls the shape of a characteristic 'spoon' or 'lollipop', where the handle and the head would correspond to the rod-like and multi-branched domains, respectively. The average measured length of PLMVd-*ml*(+)wt was 34 nm (Table 2), being the head imaged as a 15 × 20 nm ellipse (Suppl. **Fig. S4**) with a height exceeding 1.4 nm. Renaturation of PLMVd-*ml*(+)wt RNA in the folding buffer containing 4 mM Mg^{2+} rendered an overall topology where the

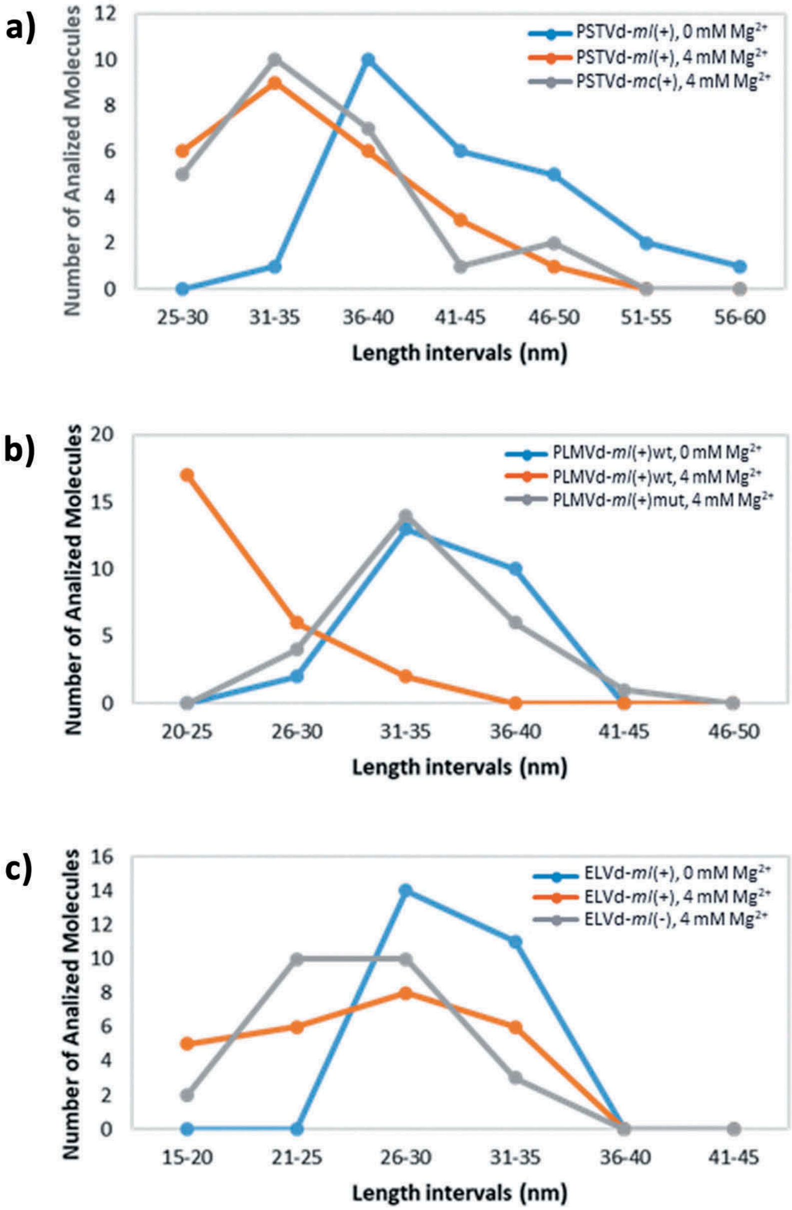

Figure 4. **Length distribution of the imaged single molecules of PSTVd (A), PLMVd (B) and ELVd (C) at 0 and 4 mM Mg^{2+}.** Length intervals of 5 nm have been used for the comparative analysis of all the viroid variants.

'spoon' shape was less evident (Fig. 6 and Suppl. **Fig. S5**), showing a marked reduction in the average length (24 nm). This Mg^{2+}-induced compaction could result from the stabilization afforded to the whole RNA structure and, particularly, to the kissing-loop interaction.

Interestingly, after renaturation in the folding buffer supplemented with 4 mM Mg^{2+} of PLMVd-*ml*(+)mut, in which the kissing-loop interaction was disrupted, the AFM analysis showed morphologies intermediate with respect to the two previous samples (Fig. 7 and Suppl. **Fig. S6**). Also, its computed average length was 33 nm, a 37.5% longer than that of PLMVd-*ml*(+)wt RNA renatured under the same Mg^{2+} concentration. Therefore, thanks to the detailed analysis performed and the high AFM resolution achieved, this study provides direct physical evidence on the stabilizing effects produced by a kissing-loop interaction in the overall 3D structure of PLMVd (+) RNA.

The size distribution of the imaged variants of PLMVd (Suppl. **Figs. S4 to S6**) depicted in Fig. 4B shows that the peak in the graph shifts to shorter lengths (20–25 nm) at 4 mM Mg^{2+} only in PLMVd-*ml*(+)wt, in which the kissing-loop interaction is allowed. In turn, the length distribution of variant PLMVd-*ml* (+)mut (with the kissing-loop interaction disrupted) at 4 mM Mg^{2+} shows a maximum in the 31–35 nm interval, as in PLMVd-*ml*(+)wt in a folding buffer lacking divalent ions. This observation reinforces the role played by the kissing-loop interaction in the stabilization of the 3D structure of PLMVd.

Eggplant latent viroid (family Avsunviroidae): similar conformations adopted by either polarity strand

Regarding ELVd, the predicted secondary structures of either polarity contain two terminal bifurcations that interrupt the overall elongated shape of the molecule. Representative AFM

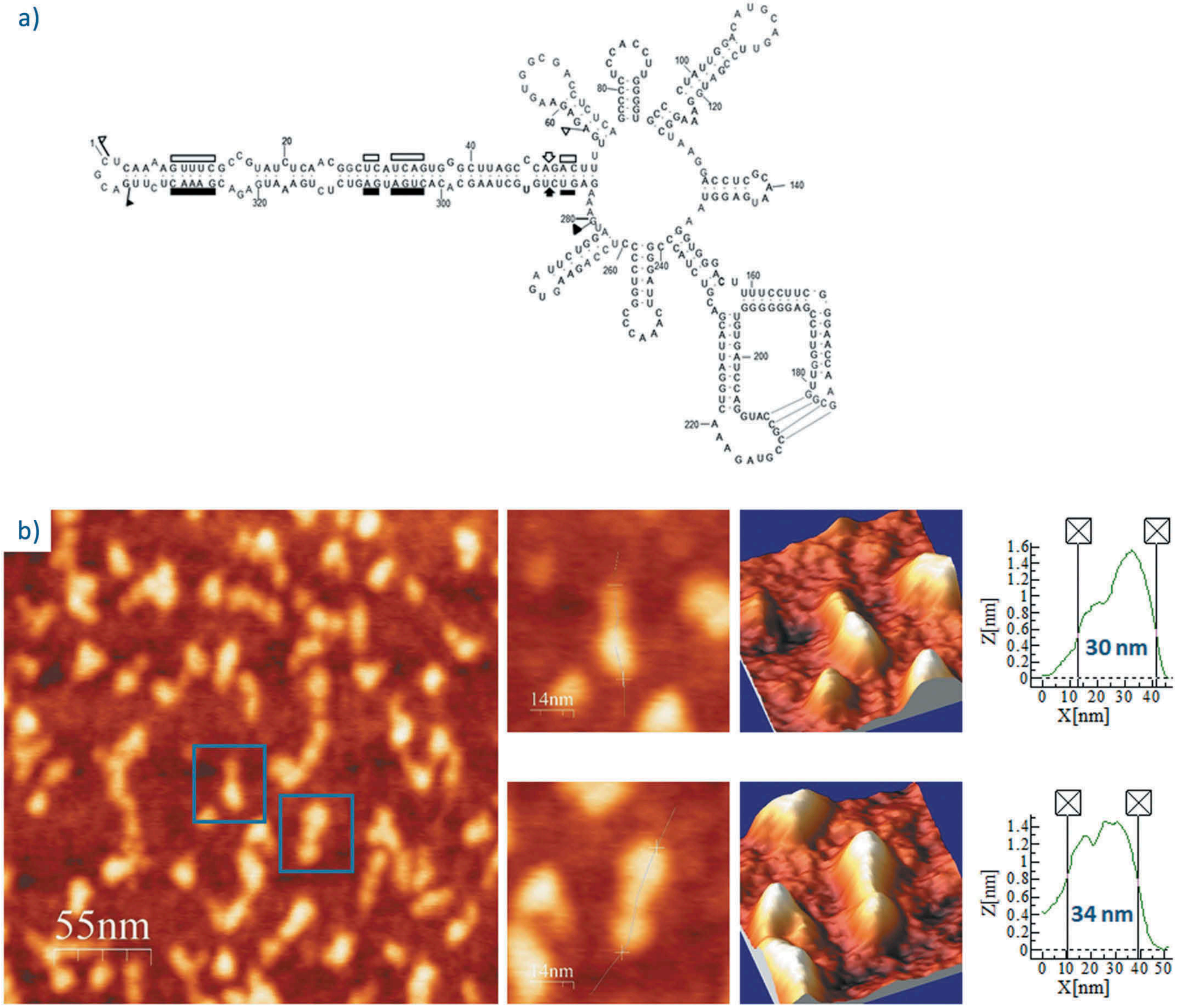

Figure 5. (A) Predicted secondary structure of PLMVd-*ml*(+)wt. The 337-nt, multibranched secondary structure of this ribozyme-containing member of the family *Avsunviroidae* is depicted. Boundaries of the (+) and (-) self-cleaving domains are indicated by flags, nucleotides conserved in most natural hammerhead structures are marked by bars, and the self-cleavage sites are identified by arrows. Filled and open symbols refer to (+) and (-) polarities, respectively. Nucleotides involved in a kissing-loop interaction supported by chemical probing [34] are identified by broken lines. Adapted from [78]. **(B) AFM images of PLMVd-*ml*(+)wt renatured in the absence of Mg^{2+}**. A field of 275 × 275 nm is shown on the left panel and two characteristic molecules are zoomed on the right. 3D views of the imaged viroid RNAs, as well as profiles with their measured lengths are also displayed.

images of ELVd-*ml*(+), the *ml* (+) RNA (see secondary structure in Fig. 8A), renatured in the buffer without Mg^{2+}, are shown in Fig. 8B and Suppl. **Fig. S7**. The topographic images reflect a majority of molecules with rod-like conformations, typically containing two or three aligned bumps, with an average length of 30 nm and a height lower than 1 nm (Table 2). ELVd-*ml*(+) was also imaged after being refolded in 4 mM Mg^{2+} and, as illustrated in Fig. 9 and Suppl. **Fig. S8**, this RNA maintained its main overall shape seen in the absence of divalent cations, though adopting a more compact conformation with one or two bumps and an average length of 26 nm, which correlated with the thickening (up to 10 nm wide and 3 nm high) observed in one of its terminal domains.

Finally, ELVd-*ml*(-), the *ml* (-) RNA (see secondary structure in Fig. 10A), was imaged after refolding in the 4 mM Mg^{2+}-containing buffer. As shown in Fig. 10B and Suppl. **Fig. S9**, the topology of the analyzed ELVd-*ml*(-) molecules was highly similar to that of ELVd-*ml*(+), with an average length of 25 nm (almost identical to that of ELVd-*ml*(+) in the same buffer), though slightly thicker in some of the imaged molecules. Therefore, AFM imaging did not reveal relevant differences in the conformation of ELVd RNAs of either polarity in 4 mM Mg^{2+}.

The size distribution of the imaged variants of ELVd (depicted in Suppl. **Figs. S7 to S9**) is summarized in Fig. 4C. For this viroid, the maximum number of individual molecules analyzed lies in the interval 26–30 nm, both in

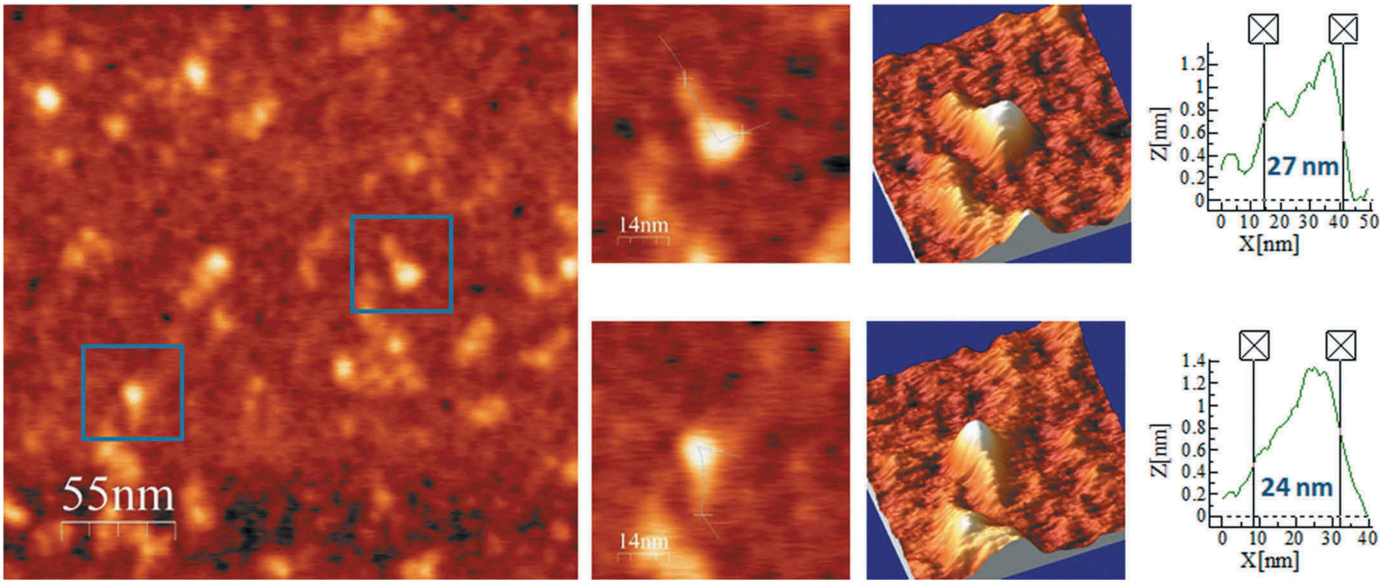

Figure 6. AFM images of PLMVd-*ml*(+)wt renatured in 4 mM Mg^{2+}. A field of 275 × 275 nm is shown on the left panel and two characteristic molecules are zoomed on the right. 3D views of the imaged viroid RNAs, as well as profiles with their measured lengths are also displayed.

ELVd-*ml*(+) (at 0 mM Mg^{2+} and 4 mM Mg^{2+}) and ELVd-*ml* (-) (at 4 mM Mg^{2+}). However, in the presence of divalent cations, the overall distribution is slightly displaced towards shorter lengths in either viroid polarity.

Discussion

Because viroid RNAs do not code for any protein, the 3D conformation they adopt plays a critical role in the expression of their biological activity [20,21]. Dissection of viroid RNA structure has been previously addressed with three methodologies. First, *in silico*, by predicting the most stable secondary structure using RNA folding algorithms [55–57]. Second, *in vitro*, by biochemical examination in solution with bisulphite, RNases, dimethyl sulphate [23,24,34] and selective 2′-hydroxyl acylation analyzed by primer extension (SHAPE) [25,58,59], as well as by biophysical approaches like nuclear magnetic resonance [60,61], thermal denaturation and temperature gradient gel electrophoresis [22,62–66] and Raman spectroscopy [67]. And third, *in vivo*, by searching for natural co-variations (and conversions of canonical into wobble base-pairs, or vice versa) that maintain the double-stranded stems [54,59,68–71], and for substitutions that preserve loop shapes in accordance with isostericity matrices predicting recurrent 3D motifs [27–29], as well as by SHAPE *in situ* with viroid-infected tissues [26,72]. However, all these techniques analyze samples composed of a very large ensemble of RNA molecules and generate average responses. In contrast, TEM (and more recently AFM, which provides 3D information) operate the other way around: they focus on isolated RNA molecules present in a given sample, and extract single-molecule information, from which individual shapes and sizes can be obtained to generate then average values. Both population-based and high-resolution single-molecule approaches are to a good extent complementary, and their combined data should strengthen the biological significance of the resulting inferences.

PSTVd, the first viroid identified and sequenced [22,23], has become the model for most studies, including its initial visualization by TEM. Under native conditions, TEM showed that the PSTVd *mc* (+) RNA (359 nt) folds into a rod-shaped conformation resembling that of a dsRNA of ~50 nm [37,38,40], while another viroid of the same family but slightly smaller (303 nt) adopts a similar conformation of ~35 nm in length [39]. These molecular sizes are consistent with each other, with that predicted theoretically for PSTVd assuming a uniform A-dsRNA conformation (49 nm), and with that first reported here by AFM for the PSTVd *ml* (+) RNA in the folding buffer lacking Mg^{2+} (43 nm). In the corresponding images, three bumps are clearly distinguishable (Fig. 1B and Suppl. **Fig. S1**), making it tempting to associate them with domains T_L+P, C and V+ T_R, respectively (see legend of Fig. 1), though more AFM-based data are needed to deepen into the PSTVd internal structure. Addition of 4 mM Mg^{2+} to the folding buffer resulted in a similar size contraction for the PSTVd-*ml*(+) and PSTVd-*mc*(+) RNAs, as expected for the shielding exerted by this cation on the repulsion between proximal negatively-charged phosphate groups of the RNA backbone. Indeed, thermal denaturation analysis has revealed that the melting temperature of viroid RNAs increases in the presence of Mg^{2+} [66].

Remarkably, in the absence of Mg^{2+}, AFM provided for PLMVd-*ml*(+)wt a different conformation resembling a ‘spoon’ or ‘lollipop’ rather than a rod. This conformation is in excellent agreement with that initially predicted *in silico* [31,54] and then *in vitro* using distinct biochemical approaches, which additionally revealed the existence of a kissing-loop interaction stabilizing the multibranched domain of this RNA (Fig. 5A) [34,36,69,71,73]. A similar though more compact topology was observed by renaturing PLMVd-*ml*(+)wt in the presence of 4 mM Mg^{2+}, showing a neat overall size reduction consistent with the stabilization of the kissing-loop exerted by the divalent cation. However, the resolution of this first AFM analysis of viroid structure is not sufficient to statistically correlate the shortening of the molecule with an increase in the diameter of

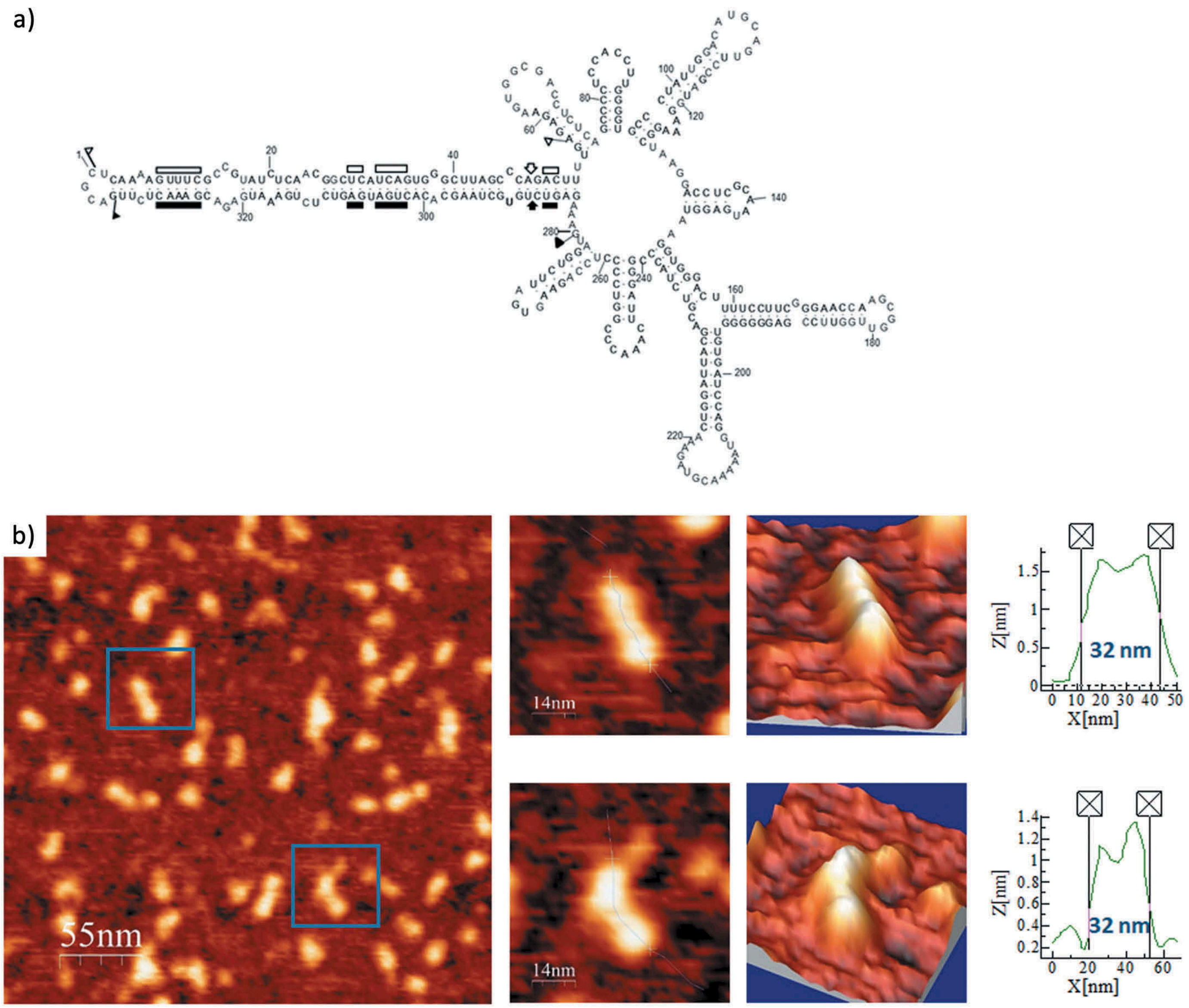

Figure 7. **(A) Predicted secondary structure of PLMVd-*ml*(+)mut, with mutations that disrupt the kissing-loop interaction characteristic of PLMVd-*ml*(+)wt.** The 337-nt, multibranched secondary structure of this mutant viroid is depicted (see details in legend of Figure 5A). **(B) AFM images of PLMVd-*ml*(+)mut renatured in 4 mM Mg^{2+}**. A field of 275 × 275 nm is shown on the left panel and two characteristic molecules are zoomed on the right. 3D views of the imaged viroid RNAs, as well as profiles with their measured lengths are also displayed.

the imaged ‘spoon head’, and/or with the reorientation of the stem-loops and hairpins forming the multibranched domain delimited by nucleotides 53–284 of PLMVd-*ml*(+)wt, a topic that deserves further investigation.

Interestingly, in the 4 mM Mg^{2+}-containing buffer, the length of the mutant PLMVd-*ml*(+)mut (with the kissing-loop interaction disrupted, see secondary structure in Fig. 7A) was significantly longer (as revealed by an ANOVA test) than that of PLMVd-*ml*(+)wt under the same ionic conditions (see Table 2 and Fig. 4B), and the ‘spoon’ conformation was clearer than in the wild-type viroid RNA under the same ionic conditions. Also, a detailed analysis of the individual PLMVd-*ml*(+)mut molecules imaged (Suppl. **Fig. S6** and data not shown), evidenced a short (10 to 15 nm long) and flat arm protruding from the head of some molecules, which might correspond to one of the hairpins of the multibranched domain in the absence of the kissing-loop interaction (Fig. 7A). Such feature was much less evident in the wild type variant PLMVd-*ml*(+)wt at 4 mM Mg^{2+} (Suppl. **Fig. S5**), as shown in the representative molecules imaged in Fig. 11. These observations highlight the relevance of elements of tertiary structure, like kissing-loop interactions that are characteristically strengthened by Mg^{2+}, in enhancing the compactness of the 3D structure of some viroid RNAs. Moreover, the results shown here are consistent with previous observations by non-denaturing PAGE showing that disruption of the kissing-loop interaction in the other viroid of the same genus results in a relaxed conformation with slower electrophoretic mobility [35].

Lastly, previous analyzes *in silico, in vitro* and *in vivo* predicted for ELVd *ml* (+) and (-) RNAs similar structures

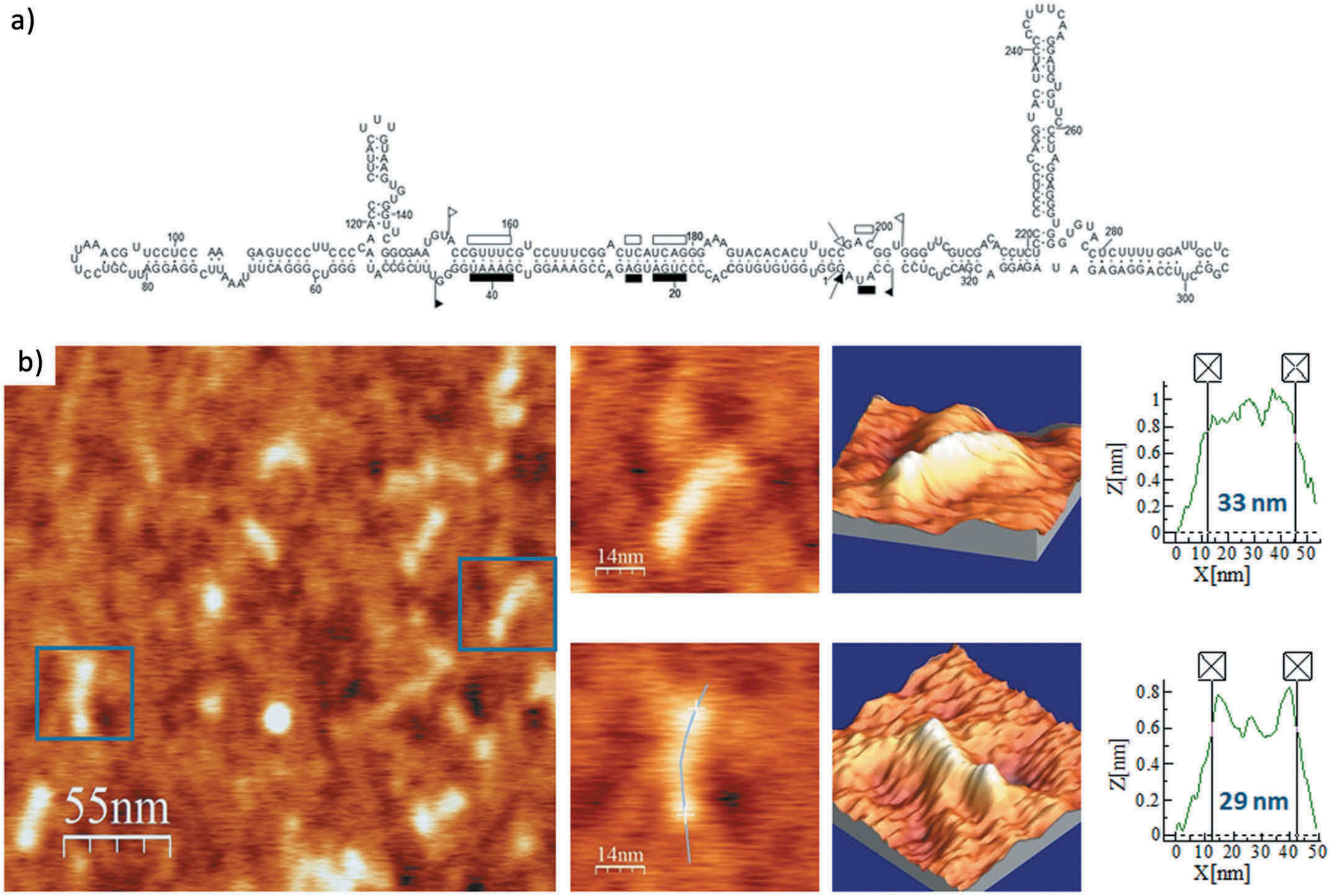

Figure 8. **(A) Predicted secondary structure of ELVd-*ml*(+).** In this ribozyme-containing member (335 nt) of the family *Avsunviroidae* the sequences involved in the hammerhead structures are delimited by flags, motifs conserved in natural hammerhead structures are denoted by bars, and self-cleavage sites are marked by arrows. Adapted from [32]. **(B) AFM images of ELVd-*ml*(+) renatured in the absence of Mg^{2+}.** A field of 275 × 275 nm is shown on the left panel and two characteristic molecules are zoomed on the right. 3D views of the imaged viroid RNAs, as well as profiles with their measured lengths are also displayed.

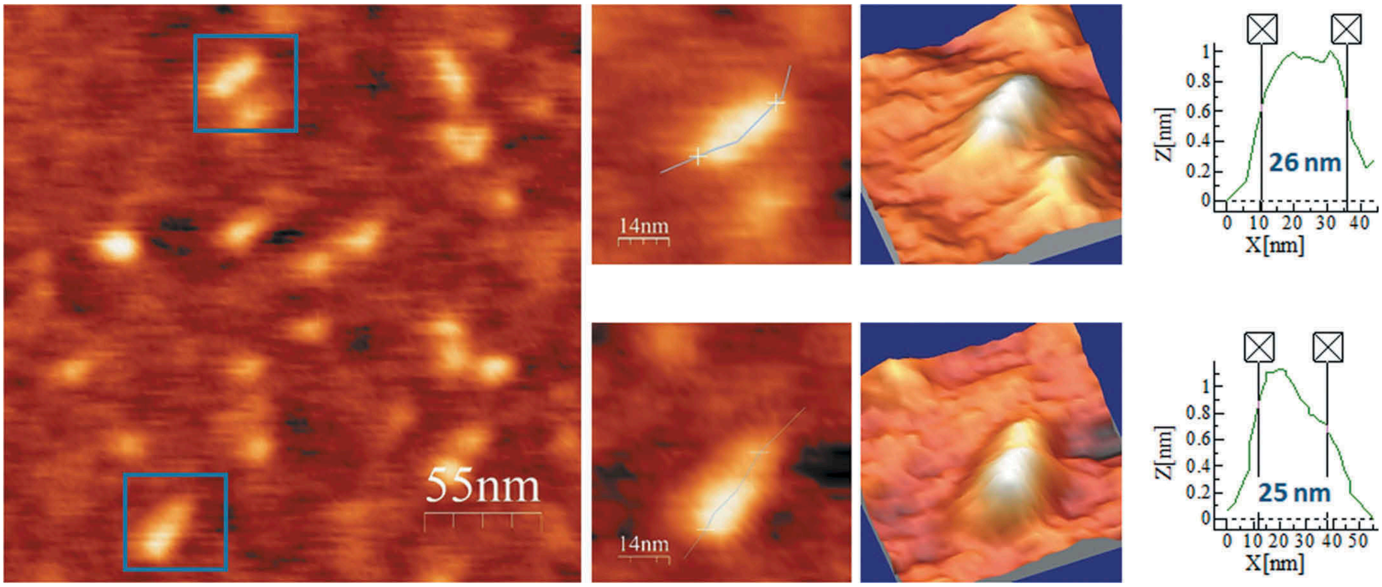

Figure 9. **AFM images of ELVd-*ml*(+) renatured in 4 mM Mg^{2+}.** A field of 275 × 275 nm is shown on the left panel and two characteristic molecules are zoomed on the right. 3D views of the imaged viroid RNAs, as well as profiles with their measured lengths are also displayed.

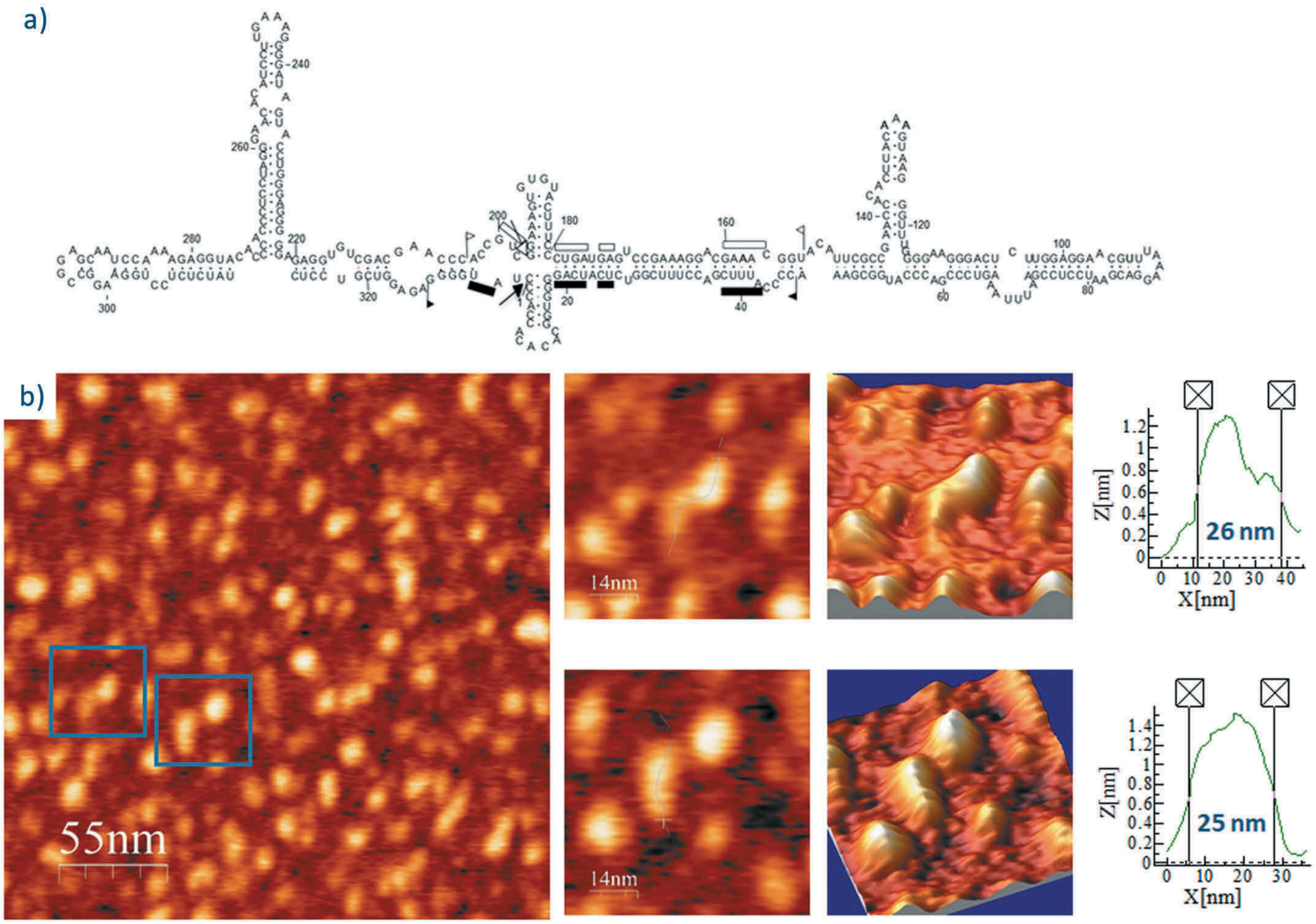

Figure 10. **(A) Predicted secondary structure of ELVd-*ml*(-)**. For details, see legend of Fig. 7A. **(B) AFM images of ELVd-*ml*(-) renatured in 4 mM Mg^{2+}**. A field of 275 × 275 nm is shown on the left panel and two characteristic molecules are zoomed on the right. 3D views of the imaged viroid RNAs, as well as profiles with their measured lengths are also displayed.

with terminal bifurcations of different size [32,58,59], somehow halfway between those reported for PSTVd-*ml*(+) (rod-like) and PLMVd-*ml*(+)wt (multibranched). Our AFM images of ELVd-*ml*(+) and ELVd-*ml*(-) are consistent with these predictions, showing comparable topology and size for either polarity strand of ELVd in Mg^{2+}-containing buffer. Moreover, in the AFM images of some of the individual molecules, a sort of thickening in one of the terminal domains was observed that could be produced by one of the bifurcations of either polarity RNA, although even at the maximum AFM resolution no clearer distinction could be made.

In summary, the AFM data reported here support and complement, using a single-molecule approach, those previously obtained with other approaches *in silico, in vitro* and *in vivo*. Although for reasons stated before [59] the latter three approaches should not necessarily concord with each other when applied to any RNA in general, they do provide consistent results when dealing with three different viroids: PSTVd, ELVd, and avocado sunblotch viroid (ASBVd), the type member of the family *Avsunviroidae* [26,59,72]. Moreover, the main conclusion from two of these studies performed by *in vivo* SHAPE is that PSTVd and ASBVd RNAs accumulate *in planta* as free RNAs, adopting a rod-shaped secondary structure without tightly-bound host proteins. Thus, the potential distorting effects that the latter might exert on viroid RNA structure *in vivo* can be reasonably dismissed and, consequently, our AFM data obtained *in vitro* for the six viroid RNA variants analyzed can be fairly extrapolated to the *in vivo* habitat. To conclude, our results provide the first direct visualization at single-molecule resolution of viroid RNA 3D structure, and confirm the stabilizing role that elements of tertiary structure, like kissing-loop interactions, play in some of their functional conformations.

Materials and methods

Viroid samples

The viroid variants analyzed by AFM in this work are listed in Table 1. PLMVd (variant gds6, GenBank AJ005303.1) and ELVd (reference variant, GenBank AJ536613) *ml* RNAs of (+), or (+) and (-) polarities, respectively, were the unit-length self-cleavage products resulting from *in vitro* transcription (under the control of the T7 or T3 promoters [74]) of recombinant plasmids containing dimeric head-to-tail viroid-cDNA inserts. PSTVd (variant RG1, GenBank U23058.1) was made to contain flanking ribozymes [15] in order to generate during *in vitro* transcription *ml* (+) RNA opened between

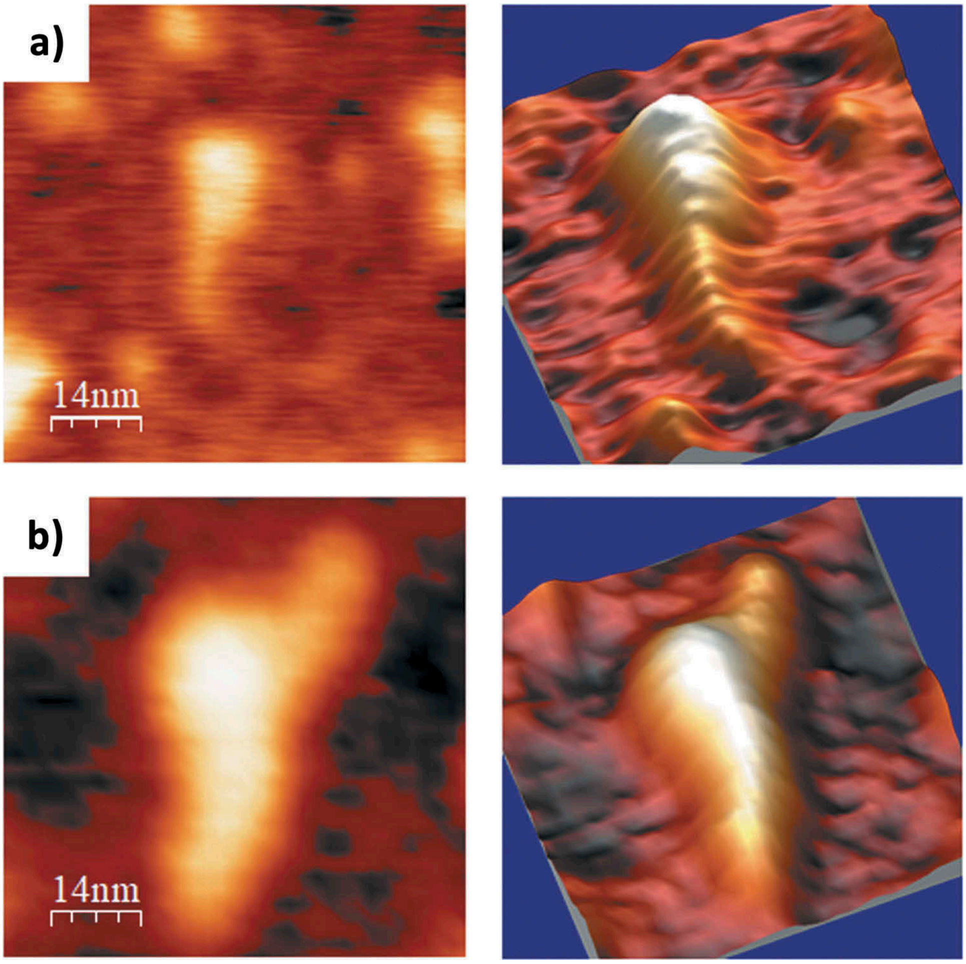

Figure 11. AFM images of selected PLMVd-*ml*(+)wt (A) and PLMVd-*ml*(+)mut (B) molecules, renatured in 4 mM Mg^{2+}. 2D (left) and 3D (right) views are displayed, which clearly show the difference in compactness among the wild type (see secondary structure in Fig. 5A) and mutant (see secondary structure in Fig. 7A) viroid RNAs, as well as the presence of a short and flat arm protruding from the head of the latter.

positions C1 and G2. A mutated version of the PLMVd-gds6 variant, with positions 209–212 (CCGC) replaced by four consecutive As, was obtained by PCR and abutted primers, one of which containing the changes to be introduced in its 5′ terminus. The unit-length strands were purified by denaturing polyacrylamide gel electrophoresis (PAGE) in 5% gels and subsequent elution. The *mc* (+) RNA of variant PSTVd-Nb (GenBank AJ634596.1) was isolated and purified from leaves of infected *Nicotiana benthamiana* by extraction with phenol-saturated buffer, fractionation with non-ionic cellulose, clarification with methoxyethanol, and double PAGE as reported before [26].

Sample preparation for AFM

Disks of muscovite mica Hi-Grade V2 (Monocomp Instrumentation) were attached to 13-mm steel pucks using Aron Alpha high-strength rapid bonding adhesive based on alpha cyanoacrylate (Agar Scientific Limited). Immediately prior to APTES functionalization, the top layer of the mica was cleaved using Scotch tape to reveal an atomically flat surface. Afterwards, the mica surface was treated with a 0.1% solution of APTES (SIGMA-Aldrich) for 15 min, washed with 2-propanol, rinsed with ultrapure, DEPC-treated milliQ water and dried at 37°C.

Purified viroid RNAs were diluted to 0.5 ng/µl in folding buffer (100 mM HEPES pH 7.4 and 100 mM NaCl), either magnesium-free or containing 4 mM $MgCl_2$. They were then denatured by incubation at 95°C for 10 min, and renatured at 37°C for 10 min. Droplets (30 µl) of renatured viroid RNAs at 1–3 nM were deposited onto freshly cleaved, APTES-modified mica surfaces and incubated at 25°C for 20 min in a humidity chamber. Excess of RNA was rinsed off with DEPC-treated MilliQ water. The RNA-containing surfaces were then air-dried at a constant temperature of 25°C for 2 h [49,50,75].

AFM imaging

AFM analysis was performed in air, at room temperature, in the dynamic mode with a Nanoscope IIIA (Veeco) and an Agilent 5500 PicoPlus (Agilent Technologies) microscopes. Tapping mode AFM was carried out using silicon cantilevers with nominal curvature radius of 8 nm (Bruker), nominal force constant of 4 N/m and resonance frequency in the 50–80 kHz range. The set-points used were kept in the 0.3–0.6 V range, while the free amplitude values were in the 0.7–0.8 V range. The images (from 512 × 512 up to 2048 × 2048 pixels) were recorded at a scan rate of 1 line/s. A minimum of three independent samples of each viroid preparation at each buffer composition (nine in total) were used, thus rendering more than 27 samples analyzed by AFM, from which different AFM fields were imaged.

The influence of the tip radius is a relevant issue when imaging nanometer structures by AFM. In principle, with a nominal tip radius of 8 nm (which is considered the optimal one for imaging biological samples in air using tapping mode, and consequently selected for this work), distances below this value are difficult to resolve. Furthermore, for larger distances tip convolution is still present and leads to a widening of the imaged structure. This later aspect has indeed been taken into account here, since the length distances have been measured between points located at half of the height of the imaged structure (as an example, see graphs in Figs. 1–3 and 5–10). This procedure leaves out of the measurement approximately 8 nm (the tip nominal radius) of lateral extension at each of both extremes of the imaged molecule, thus minimizing the tip size effects.

Image analyses

The software package WSxM v5.0 (Nanotec) [76] was used to analyze all the AFM images, as well as to measure the length of 25 individual, full-length viroid RNA molecules that were randomly chosen among those present in different samples of each preparation. The selection of full-length molecules (using broad enough intervals of 25–60 nm in PSTVd, 20–50 nm in PLMVd and 15–40 nm in ELVd, see Fig. 4), which showed the viroid morphology characteristic of each species, excluded: i) shorter RNAs likely resulting from Mg^{2+}-induced cleavage, ii) RNAs showing unusual molecular orientations on the modified mica surface, and iii) longer structures likely generated by bimolecular complexes or multimeric RNA aggregates.

Abbreviations

AFM	atomic force microscopy
APTES	3-aminopropyltriethoxysilane
ASBVd	avocado sunblotch viroid
CCR	central conserved region
ELVd	eggplant latent viroid
mc and *ml*	monomeric circular and linear viroid RNA, respectively
PAGE	polyacrylamide gel electrophoresis
PLMVd	peach latent mosaic viroid
PSTVd	potato spindle tuber viroid
SHAPE	selective 2′-hydroxyl acylation analyzed by primer extension
TEM	transmission electron microscopy

Disclosure of Potential Conflicts of Interest

No potential conflicts of interest were disclosed.

Funding

This work was supported by the Spanish Ministerio de Economía y Competitividad (MINECO) grants BIO2016-79618-R (funded by EU under the FEDER programme) to C.B. and BFU2104-56812-P to R.F., as well as by the Comunidad de Madrid grant S2018/NMT-4349 to L.V. CIBERehd is funded by the Instituto de Salud Carlos III (ISCIII).

ORCID

M. Moreno http://orcid.org/0000-0002-6065-4095
L. Vázquez http://orcid.org/0000-0001-6220-2810
A. López-Carrasco http://orcid.org/0000-0001-9202-2597
J.A. Martín-Gago http://orcid.org/0000-0003-2663-491X
R. Flores http://orcid.org/0000-0002-3033-5077
C. Briones http://orcid.org/0000-0003-2213-8353

References

[1] Diener TO. Discovering viroids–a personal perspective. Nat Rev Microbiol. 2003 Oct;1(1):75–80.PubMed PMID: 15040183

[2] Flores R, Hernandez C, Martinez de Alba AE, et al. Viroids and viroid-host interactions. Annu Rev Phytopathol. 2005;43:117–139. PubMed PMID: 16078879

[3] Ding B. The biology of viroid-host interactions. Annu Rev Phytopathol. 2009;47:105–131. PubMed PMID: 19400635

[4] Zhang Z, Qi S, Tang N, et al. Discovery of replicating circular RNAs by RNA-seq and computational algorithms. PLoS Pathog. 2014 Dec;10(12):e1004553. PubMed PMID: 25503469; PubMed Central PMCID: PMCPMC4263765.

[5] Serra P, Messmer A, Sanderson D, et al. Apple hammerhead viroid-like RNA is a bona fide viroid: autonomous replication and structural features support its inclusion as a new member in the genus Pelamoviroid. Virus Res. 2018 Apr2;249:8–15. PubMed PMID: 29510173.

[6] Hadidi A, Flores R, Randles JW, et al. editors. Viroids and Satellites. Boston: Academic Press; 2017.

[7] Flores R, Minoia S, Carbonell A, et al. Viroids, the simplest RNA replicons: how they manipulate their hosts for being propagated and how their hosts react for containing the infection. Virus Res. 2015 Nov2;209:136–145. PubMed PMID: 25738582.

[8] Hammann C, Steger G. Viroid-specific small RNA in plant disease. RNA Biol. 2012 Jun;9(6):809–819. PubMed PMID: 22617880

[9] Kovalskaya N, Hammond RW. Molecular biology of viroid-host interactions and disease control strategies. Plant Sci. 2014 Nov;228:48–60. PubMed PMID: 25438785.

[10] Tsagris EM, Martinez de Alba AE, Gozmanova M, et al. Viroids. Cell Microbiol. 2008 Nov;10(11):2168–2179. PubMed PMID: 18764915.

[11] Grill LK, Semancik JS. RNA sequences complementary to citrus exocortis viroid in nucleic acid preparations from infected gynura aurantiaca. Proc Natl Acad Sci U S A. 1978 Feb;75(2):896–900. PubMed PMID: 16592500; PubMed Central PMCID: PMCPMC411364

[12] Branch AD, Benenfeld BJ, Robertson HD. Evidence for a single rolling circle in the replication of potato spindle tuber viroid. Proc Natl Acad Sci U S A. 1988 Dec;85(23):9128–9132. PubMed PMID: 16594003; PubMed Central PMCID: PMCPMC282677

[13] Branch AD, Robertson HD. A replication cycle for viroids and other small infectious RNA's. Science. 1984 Feb 3;223 (4635):450–455. PubMed PMID: 6197756

[14] Daros JA, Marcos JF, Hernandez C, et al. Replication of avocado sunblotch viroid: evidence for a symmetric pathway with two rolling circles and hammerhead ribozyme processing. Proc Natl Acad Sci U S A. 1994 Dec 20;91(26):12813–12817. PubMed PMID: 7809126; PubMed Central PMCID: PMCPMC45530

[15] Feldstein PA, Hu Y, Owens RA. Precisely full length, circularizable, complementary RNA: an infectious form of potato spindle tuber viroid. Proc Natl Acad Sci U S A. 1998 May 26;95 (11):6560–6565. PubMed PMID: 9601006; PubMed Central PMCID: PMCPMC27879

[16] Daros JA, Flores R. Arabidopsis thaliana has the enzymatic machinery for replicating representative viroid species of the family Pospiviroidae. Proc Natl Acad Sci U S A. 2004 Apr 27;101(17):6792–6797. PubMed PMID: 15096616; PubMed Central PMCID: PMCPMC404124.

[17] Flores R, Gago-Zachert S, Serra P, et al. Viroids: survivors from the RNA world? Annu Rev Microbiol. 2014;68:395–414. PubMed PMID: 25002087

[18] Diener TO. Circular RNAs: relics of precellular evolution? Proc Natl Acad Sci U S A. 1989 Dec;86(23):9370–9374. PubMed PMID: 2480600; PubMed Central PMCID: PMCPMC298497

[19] Ruiz-Mirazo K, Briones C, de la Escosura A. Prebiotic systems chemistry: new perspectives for the origins of life. Chem Rev. 2014 Jan 8;114(1):285–366. PubMed PMID: 24171674.

[20] Flores R, Serra P, Minoia S, et al. Viroids: from genotype to phenotype just relying on RNA sequence and structural motifs. Front Microbiol. 2012;3:217. PubMed PMID: 22719735; PubMed Central PMCID: PMCPMC3376415

[21] Steger G, Perreault JP. Structure and associated biological functions of viroids. Adv Virus Res. 2016;94: 141–172. 2016/03/22 ed.

[22] Diener TO. Potato spindle tuber viroid. 8. Correlation of infectivity with a UV-absorbing component and thermal denaturation properties of the RNA. Virology. 1972 Nov;50(2):606–609. PubMed PMID: 4636118

[23] Gross HJ, Domdey H, Lossow C, et al. Nucleotide sequence and secondary structure of potato spindle tuber viroid. Nature. 1978 May 18;273(5659):203–208. PubMed PMID: 643081

[24] Gast FU, Kempe D, Spieker RL, et al. Secondary structure probing of potato spindle tuber viroid (PSTVd) and sequence comparison with other small pathogenic RNA replicons provides evidence for central non-canonical base-pairs, large A-rich loops, and a terminal branch. J Mol Biol. 1996 Oct 11;262(5):652–670. PubMed PMID: 8876645.

[25] Giguere T, Adkar-Purushothama CR, Perreault JP. Comprehensive secondary structure elucidation of four genera of the family *Pospiviroidae*. PLoS One. 2014;9(6):e98655. PubMed PMID: 24897295; PubMed Central PMCID: PMCPMC4045682

[26] Lopez-Carrasco A, Flores R. Dissecting the secondary structure of the circular RNA of a nuclear viroid in vivo: A “naked” rod-like conformation similar but not identical to that observed in vitro. RNA Biol. 2017 Aug 3;14(8):1046–1054. PubMed PMID: 27574720; PubMed Central PMCID: PMCPMC5680722.

[27] Wang Y, Zirbel CL, Leontis NB, et al. RNA 3-dimensional structural motifs as a critical constraint of viroid RNA evolution. PLoS Pathog. 2018 Feb;14(2):e1006801. PubMed PMID: 29470541; PubMed Central PMCID: PMCPMC5823408.

[28] Zhong X, Leontis N, Qian S, et al. Tertiary structural and functional analyses of a viroid RNA motif by isostericity matrix and mutagenesis reveal its essential role in replication. J Virol. 2006 Sep;80(17):8566–8581. PubMed PMID: 16912306; PubMed Central PMCID: PMCPMC1563885.

[29] Zhong X, Tao X, Stombaugh J, et al. Tertiary structure and function of an RNA motif required for plant vascular entry to initiate systemic trafficking. Embo J. 2007 Aug 22;26(16):3836–3846. PubMed PMID: 17660743; PubMed Central PMCID: PMCPMC1952227.

[30] Zhong X, Archual AJ, Amin AA, et al. A genomic map of viroid RNA motifs critical for replication and systemic trafficking. Plant Cell. 2008;20(1):35–47.

[31] Hernandez C, Flores R. Plus and minus RNAs of peach latent mosaic viroid self-cleave in vitro via hammerhead structures. Proc Natl Acad Sci U S A. 1992 May 1;89(9):3711–3715. PubMed PMID: 1373888; PubMed Central PMCID: PMCPMC525560

[32] Fadda Z, Daros JA, Fagoaga C, et al. Eggplant latent viroid, the candidate type species for a new genus within the family *Avsunviroidae* (hammerhead viroids). J Virol. 2003 Jun;77(11):6528–6532. PubMed PMID: 12743309; PubMed Central PMCID: PMCPMC155007

[33] Navarro B, Flores R. Chrysanthemum chlorotic mottle viroid: unusual structural properties of a subgroup of self-cleaving viroids with hammerhead ribozymes. Proc Natl Acad Sci U S A. 1997 Oct 14;94(21):11262–11267. PubMed PMID: 9326597; PubMed Central PMCID: PMCPMC23434

[34] Bussiere F, Ouellet J, Cote F, et al. Mapping in solution shows the peach latent mosaic viroid to possess a new pseudoknot in a complex, branched secondary structure. J Virol. 2000 Mar;74(6):2647–2654. PubMed PMID: 10684279; PubMed Central PMCID: PMCPMC111753

[35] Gago S, De la Pena M, Flores R. A kissing-loop interaction in a hammerhead viroid RNA critical for its *in vitro* folding and *in vivo* viability. Rna. 2005 Jul;11(7):1073–1083. PubMed PMID: 15928342; PubMed Central PMCID: PMCPMC1370792

[36] Dubé A, Baumstark T, Bisaillon M, et al. The RNA strands of the plus and minus polarities of peach latent mosaic viroid fold into different structures. Rna. 2010 Mar;16(3):463–473. PubMed PMID: 20089682; PubMed Central PMCID: PMCPMC2822911

[37] Sogo JM, Koller T, Diener TO. Potato spindle tuber viroid. X. Visualization and size determination by electron microscopy. Virology. 1973 Sep;55(1):70–80. PubMed PMID: 4728831

[38] Goodman TC, Nagel L, Rappold W, et al. Viroid replication: equilibrium association constant and comparative activity measurements for the viroid-polymerase interaction. Nucleic Acids Res. 1984 Aug 10;12(15):6231–6246. PubMed PMID: 6473106; PubMed Central PMCID: PMCPMC320069

[39] Sanger HL, Klotz G, Riesner D, et al. Viroids are single-stranded covalently closed circular RNA molecules existing as highly base-paired rod-like structures. Proc Natl Acad Sci U S A. 1976 Nov;73(11):3852–3856. PubMed PMID: 1069269; PubMed Central PMCID: PMCPMC431239

[40] McClements WL, Kaesberg P. Size and secondary structure of potato spindle tuber viroid. Virology. 1977 Feb;76(2):477–484. PubMed PMID: 841846

[41] Bustamante C, Keller D. Scanning force microscopy in biology. Physics Today. 1995;48(12):32–38.

[42] Hansma HG, Kasuya K, Oroudjev E. Atomic force microscopy imaging and pulling of nucleic acids. Curr Opin Struct Biol. 2004 Jun;14(3):380–385. PubMed PMID: 15193320

[43] Kuznetsov YG, Daijogo S, Zhou J, et al. Atomic force microscopy analysis of icosahedral virus RNA. J Mol Biol. 2005;347(1):41–52.

[44] Alvarez DE, Lodeiro MF, Luduena SJ, et al. Long-range RNA-RNA interactions circularize the dengue virus genome. J Virol. 2005 Jun;79(11):6631–6643. PubMed PMID: 15890901; PubMed Central PMCID: PMCPMC1112138.

[45] Schon P. Atomic force microscopy of RNA: state of the art and recent advancements. Semin Cell Dev Biol. 2018 Jan;73:209–219. PubMed PMID: 28843977.

[46] Hansma HG, Oroudjev E, Baudrey S, et al. TectoRNA and ‘kissing-loop’ RNA: atomic force microscopy of self-assembling RNA structures. J Microsc. 2003 Dec;212(Pt 3):273–279. PubMed PMID: 14629553.

[47] Basame S, Wai-Lun Li P, Howard G, et al. Spatial assembly and RNA binding stoichiometry of a LINE-1 protein essential for retrotransposition. J Mol Biol. 2006 Mar 24;357(2):351–357. PubMed PMID: 16434051.

[48] Ares P, Fuentes-Perez ME, Herrero-Galan E, et al. High resolution atomic force microscopy of double-stranded RNA [10.1039/C5NR07445B]. Nanoscale. 2016;8(23):11818–11826.

[49] Gilmore JL, Yoshida A, Takahashi H, et al. Analyses of nuclear proteins and nucleic acid structures using atomic force microscopy. In: Nakagawa S, Hirose Teditors. Nuclear bodies and noncoding RNAs: methods and protocols. New York, NY: Springer New York; 2015. p. 119–153.

[50] Garcia-Sacristan A, Moreno M, Ariza-Mateos A, et al. A magnesium-induced RNA conformational switch at the internal ribosome entry site of hepatitis C virus genome visualized by atomic force microscopy. Nucleic Acids Res. 2015 Jan;43(1):565–580. PubMed PMID: 25510496; PubMed Central PMCID: PMCPMC4288189.

[51] Cheng H, Zhang K, Libera JA, et al. Polynucleotide adsorption to negatively charged surfaces in divalent salt solutions. Biophys J.

2006 Feb 15;90(4):1164–1174. PubMed PMID: 16449197; PubMed Central PMCID: PMCPMC1367268.

[52] Lyubchenko YL, Shlyakhtenko LS, Ando T. Imaging of nucleic acids with atomic force microscopy. Methods. 2011 Jun;54 (2):274–283. PubMed PMID: 21310240; PubMed Central PMCID: PMCPMC3114274

[53] Lang D, Steely HT Jr., Kao CY, et al. Length, mass, and denaturation of double-stranded RNA molecules compared with DNA. Biochim Biophys Acta. 1987 Dec 8;910(3):271–281. PubMed PMID: 3118956

[54] Ambros S, Hernandez C, Desvignes JC, et al. Genomic structure of three phenotypically different isolates of peach latent mosaic viroid: implications of the existence of constraints limiting the heterogeneity of viroid quasispecies. J Virol. 1998 Sep;72 (9):7397–7406. PubMed PMID: 9696836; PubMed Central PMCID: PMCPMC109966

[55] Lorenz R, Bernhart SH, Honer Zu Siederdissen C, et al. ViennaRNA package 2.0 [journal article]. Algorithms Mol Biol. 2011 Nov 24;6(1):26. PubMed PMID: 22115189; PubMed Central PMCID: PMCPMC3319429.

[56] Reuter JS, Mathews DH. RNAstructure: software for RNA secondary structure prediction and analysis. BMC Bioinformatics. 2010 Mar 15;11:129. PubMed PMID: 20230624; PubMed Central PMCID: PMCPMC2984261.

[57] Zuker M. Mfold web server for nucleic acid folding and hybridization prediction. Nucleic Acids Res. 2003 Jul 1;31(13):3406–3415. PubMed PMID: 12824337; PubMed Central PMCID: PMCPMC169194

[58] Giguere T, Adkar-Purushothama CR, Bolduc F, et al. Elucidation of the structures of all members of the Avsunviroidae family. Mol Plant Pathol. 2014 Oct;15(8):767–779. PubMed PMID: 25346967

[59] Lopez-Carrasco A, Gago-Zachert S, Mileti G, et al. The transcription initiation sites of eggplant latent viroid strands map within distinct motifs in their in vivo RNA conformations. RNA Biol. 2016;13(1):83–97. PubMed PMID: 26618399; PubMed Central PMCID: PMCPMC4829332

[60] Dingley AJ, Steger G, Esters B, et al. Structural characterization of the 69 nucleotide potato spindle tuber viroid left-terminal domain by NMR and thermodynamic analysis. J Mol Biol. 2003 Dec 5;334(4):751–767. PubMed PMID: 14636600

[61] Dufour D, de la Pena M, Gago S, et al. Structure-function analysis of the ribozymes of chrysanthemum chlorotic mottle viroid: a loop-loop interaction motif conserved in most natural hammerheads. Nucleic Acids Res. 2009 Feb;37(2):368–381. PubMed PMID: 19043070; PubMed Central PMCID: PMCPMC2632901.

[62] Baumstark T, Riesner D. Only one of four possible secondary structures of the central conserved region of potato spindle tuber viroid is a substrate for processing in a potato nuclear extract. Nucleic Acids Res. 1995 Nov 11;23(21):4246–4254. PubMed PMID: 7501442; PubMed Central PMCID: PMCPMC307376

[63] Delan-Forino C, Deforges J, Benard L, et al. Structural analyses of avocado sunblotch viroid reveal differences in the folding of plus and minus RNA strands. Viruses. 2014 Jan 29;6(2):489–506. PubMed PMID: 24481250; PubMed Central PMCID: PMCPMC3939467. eng.

[64] Henco K, Sanger HL, Riesner D. Fine structure melting of viroids as studied by kinetic methods. Nucleic Acids Res. 1979 Jul 11;6 (9):3041–3059. PubMed PMID: 493134; PubMed Central PMCID: PMCPMC327916

[65] Riesner D, Henco K, Rokohl U, et al. Structure and structure formation of viroids. J Mol Biol. 1979 Sep 5;133(1):85–115. PubMed PMID: 529284

[66] Semancik JS, Morris TJ, Weathers LG, et al. Physical properties of a minimal infectious RNA (viroid) associated with the exocortis disease. Virology. 1975 Jan;63(1):160–167. PubMed PMID: 1111210

[67] Hui-Bon-Hoa G, Kaddour H, Vergne J, et al. Raman characterization of avocado sunblotchviroid and its response to external perturbations and self-cleavage [journal article]. BMC Biophys. 2014 March 21;7(1):2.

[68] De la Pena M, Navarro B, Flores R. Mapping the molecular determinant of pathogenicity in a hammerhead viroid: A tetraloop within the *in vivo* branched RNA conformation. Proc Natl Acad Sci U S A. 1999;96(17):9960–9965.

[69] Fekih Hassen I, Massart S, Motard J, et al. Molecular features of new peach latent mosaic viroid variants suggest that recombination may have contributed to the evolution of this infectious RNA. Virology. 2007 Mar 30;360(1):50–57. PubMed PMID: 17113618.

[70] Pelchat M, Levesque D, Ouellet J, et al. Sequencing of peach latent mosaic viroid variants from nine North American peach cultivars shows that this RNA folds into a complex secondary structure. Virology. 2000 May 25;271(1):37–45. PubMed PMID: 10814568.

[71] Serra P, Bertolini E, Martinez MC, et al. Interference between variants of peach latent mosaic viroid reveals novel features of its fitness landscape: implications for detection. Sci Rep. 2017 Feb17;7:42825. PubMed PMID: 28211491; PubMed Central PMCID: PMCPMC5314366.

[72] Lopez-Carrasco A, Flores R. The predominant circular form of avocado sunblotch viroid accumulates in planta as a free RNA adopting a rod-shaped secondary structure unprotected by tightly bound host proteins. J Gen Virol. 2017 Jul;98(7):1913–1922. PubMed PMID: 28699864

[73] Dube A, Bolduc F, Bisaillon M, et al. Mapping studies of the peach latent mosaic viroid reveal novel structural features. Mol Plant Pathol. 2011 Sep;12(7):688–701. PubMed PMID: 21726370; PubMed Central PMCID: PMCPMC3256235.

[74] Green MR, Sambrook J. Molecular cloning: A laboratory manual. Vol. 1. New York, NY: Cold Spring Harbor Laboratory Press; 2012.

[75] Lyubchenko Y, Shlyakhtenko L, Harrington R, et al. Atomic force microscopy of long DNA: imaging in air and under water [article]. Proc Natl Acad Sci U S A. 1993 Mar 15;90 (6):2137–2140. PubMed PMID: 8460119; PubMed Central PMCID: PMCPMC46040.

[76] Horcas I, Fernandez R, Gomez-Rodriguez JM, et al. WSXM: a software for scanning probe microscopy and a tool for nanotechnology. Rev Sci Instrum. 2007 Jan;78(1):013705. PubMed PMID: 17503926.

[77] Keese P, Symons RH. Domains in viroids: evidence of intermolecular RNA rearrangements and their contribution to viroid evolution. Proc Natl Acad Sci U S A. 1985 Jul;82(14):4582–4586. PubMed PMID: 3860809; PubMed Central PMCID: PMCPMC390429

[78] Di Serio F, Gisel A, Navarro B, et al. Deep sequencing of the small RNAs derived from two symptomatic variants of a chloroplastic viroid: implications for their genesis and for pathogenesis. PLoS One. 2009 Oct 21;4(10):e7539. PubMed PMID: 19847296; PubMed Central PMCID: PMCPMC2760764.